frontiers in Earth Science

ORIGINAL RESEARCH
published: 12 February 2021
doi: 10.3389/feart.2020.570742

Biomarker and Isotopic Composition of Seep Carbonates Record Environmental Conditions in Two Arctic Methane Seeps

Haoyi Yao[1], Giuliana Panieri[1]*, Moritz F. Lehmann[2], Tobias Himmler[1,3] and Helge Niemann[1,2,4,5]*

[1]CAGE—Centre for Arctic Gas Hydrate, Environment and Climate, Department of Geosciences, UiT the Arctic University of Norway, Tromsø, Norway, [2]Department of Environmental Sciences, University of Basel, Basel, Switzerland, [3]Geological Survey of Norway, Trondheim, Norway, [4]Department of Marine Microbiology and Biogeochemistry, NIOZ Royal Institute for Sea Research, Texel, Netherlands, [5]Department of Earth Sciences, Faculty of Geosciences, Utrecht University, Utrecht, Netherlands

Present-day activity of cold seeps in the ocean is evident from direct observations of methane emanating from the seafloor, the presence of chemosynthetic organisms, or the quantification of high gas concentrations in sediment pore waters and the water column. Verifying past cold seep activity and biogeochemical characteristics is more challenging but may be reconstructed from proxy records of authigenic seep carbonates. Here, we investigated the lipid-biomarker inventory, carbonate mineralogy, and stable carbon and oxygen isotope compositions of seep-associated carbonates from two active Arctic methane seeps, located to the northwest (Vestnesa Ridge; ~1,200 m water depth) and south (Storfjordrenna; ~380 m water depth) offshore Svalbard. The aragonite-dominated mineralogy of all but one carbonate sample indicate precipitation close to the seafloor in an environment characterized by high rates of sulfate-dependent anaerobic oxidation of methane (AOM). In contrast, Mg-calcite rich nodules sampled in sediments of Storfjordrenna appear to have formed at the sulfate-methane-transition zone deeper within the sediment at lower rates of AOM. AOM activity at the time of carbonate precipitation is indicated by the ^{13}C-depleted isotope signature of the carbonates [–20 to –30‰ Vienna Pee Dee Belemnite (VPDB)], as well as high concentrations of ^{13}C-depleted lipid biomarkers diagnostic for anaerobic methanotrophic archaea (archaeol and sn2-hydroxyarchaeol) and sulfate-reducing bacteria (iso and anteiso-C15:0 fatty acids) in the carbonates. We also found ^{13}C-depleted lipid biomarkers (diploptene and a 4α-methyl sterol) that are diagnostic for bacteria mediating aerobic oxidation of methane (MOx). This suggests that the spatial separation between AOM and MOx zones was relatively narrow at the time of carbonate formation, as is typical for high methane-flux regimes. The seep-associated carbonates also displayed relatively high δ^{18}O values (4.5–5‰ VPDB), indicating the presence of ^{18}O-enriched fluids during precipitation, possibly derived from destabilized methane gas hydrates. Based on the combined isotopic evidence, we suggest that all the seep carbonates resulted from the anaerobic oxidation of methane during intense methane seepage. The seepage likely was associated to gas hydrates destabilization, which led to the methane ebullition from the seafloor into the water column.

Keywords: gas hydrate, Arctic, seep carbonate, methane seep, lipid biomarkers

OPEN ACCESS

Edited by:
Ira Leifer, Bubbleology Research Intnl, United States

Reviewed by:
Huan Cui, Université de Paris, France
Joachim Reitner, University of Göttingen, Germany

****Correspondence:***
Haoyi Yao
haoyi.yao11@gmail.com
Giuliana Panieri
Giuliana.panieri@uit.no

Specialty section:
This article was submitted to Biogeoscience, a section of the journal Frontiers in Earth Science

Received: *08 June 2020*
Accepted: *30 December 2020*
Published: *12 February 2021*

Citation:
Yao H, Panieri G, Lehmann MF, Himmler T and Niemann H (2021) Biomarker and Isotopic Composition of Seep Carbonates Record Environmental Conditions in Two Arctic Methane Seeps. Front. Earth Sci. 8:570742. doi: 10.3389/feart.2020.570742

INTRODUCTION

Marine sediments contain large quantities of methane in the form of free- or dissolved gas, or gas hydrate. While the benthic methane reservoir is relatively stable at present, concern exists that a warmer future ocean will facilitate higher methane emission rates from the seafloor to the water column and potentially to the atmosphere (Kennet, 2000; Dickens, 2003). Gas hydrates are particularly susceptible to dissociation if bottom water heat efficiently penetrates into the seafloor (MacDonald et al., 1994; Dickens et al., 1995; Kennett, 2000; Dickens, 2003). In the Arctic Ocean, climate change causes atmospheric temperatures to increase much faster than in lower latitudes (IPCC, 2013; Bintanja, 2018). Bottom-water warming may thus be more severe in the Arctic. It may render Arctic gas hydrate deposits in sediments in shallow waters particularly vulnerable to destabilization. Knowledge of the emission history of Arctic seeps is thus crucial in order to understand how environmental parameters have affected methane emissions in the past, and in order to estimate how these will modulate methane emission in the future.

Past methane seepage can be deciphered from relicts of microbial communities that are dependent on methane, which are recorded in authigenic seep carbonates (e.g., Peckmann and Thiel, 2004). At present, most methane in ocean sediments is consumed through the microbially mediated sulfate-dependent anaerobic oxidation of methane-AOM (e.g., Reeburgh, 2007):

$$CH_4 + SO_4^{2-} \rightleftarrows HS^- + HCO_3^- + H_2O \quad (1)$$

The oxidation of methane coupled to the reduction of sulfate forms a zone in sediments, where both methane and sulfate are both consumed and this zone is known as the sulfate-methane transition zone (SMTZ). AOM is mediated by anaerobic methanotrophic archaea (ANME), typically forming syntrophic partnerships with sulfate-reducing bacteria (SRB; Knittel and Boetius, 2009). Methane bypassing the AOM filter can then be oxidized by aerobic methanotrophic bacteria (MOB) at the seafloor or in the water column (Niemann et al., 2006; Knief, 2015; James et al., 2016). At highly active gas seeps, the spatial distance between these activity horizons in the sediments, one that is dominated by AOM and the other one by MOx, can be at the centimeter or even millimeter scale (Niemann et al., 2006; Elvert and Niemann, 2008). The AOM end-products HS^- and HCO_3- result in increased alkalinity in the sediment pore waters, which facilitates precipitation of authigenic carbonates. The precipitating carbonates can then encase the methanotrophic communities that were present in the sediments at the time of their precipitation. Molecular fossils such as lipid biomarkers of aerobic and anaerobic methanotrophic microbes are typically ^{13}C-depleted because AOM, as well as MOx, strongly discriminate against methane containing the heavy isotope ^{13}C. Lipids of these communities have a high preservation potential in seep carbonates (Peckmann et al., 1999; Niemann et al., 2005; Birgel et al., 2008; Birgel et al. 2011), thus allowing to reconstruct past microbial communities at the seep site (Niemann and Elvert, 2008).

Carbonates can form nodules, slabs, crusts, chimneys and sometimes massive pavements at cold seeps (Aloisi et al., 2000; Reitner et al., 2005; Krause et al., 2017). Seep carbonates are preserved at the seafloor or within sediments even after the methane flux has diminished and thus constitute a geological record of past seepage (e.g., Peckmann and Thiel, 2004; Feng et al., 2010; Crémière et al., 2016a; Sauer et al., 2017). The mineralogy and isotopic signatures of seep carbonates, as well as its lipid biomarker inventory, can provide information on the environmental conditions and microbial communities during past seepage episodes, and potential changes of the ascending fluids over time (Argentino et al., 2019).

Because of the carbon isotope effects associated with AOM and the usually ^{13}C depleted signature of the methane substrate, seep carbonates typically display low $\delta^{13}C$ values reflecting the incorporation of predominantly methane-derived carbon (Peckmann et al., 1999; Aloisi et al., 2000; Crémière et al., 2016b; Yao et al., 2020). In contrast, the carbonate O-isotope ratios are influenced by the fluid source water; thus, the $\delta^{18}O$ values of carbonates have been used as a proxy to determine the origin of fluids with differential ^{18}O-signatures, e.g., gas hydrate derived water, water from clay dehydration, or seawater (Bohrmann et al., 1998; Aloisi et al., 2000; Han and Aizenberg, 2003; Feng et al., 2014; Dessandier et al., 2020). Finally, the mineralogy of seep carbonates (aragonite vs. calcite or dolomite) indicates whether they were formed close to the seafloor (aragonite) or rather in the deeper sediments (calcite/high-Mg and calcite/dolomite) (Bohrmann et al., 1998; Aloisi et al., 2000; Haas et al., 2010).

In this study, we investigated seep carbonates sampled from the seafloor and sediment cores obtained at two active seep sites in the Arctic Ocean with underlying gas hydrates: 1) the deepwater Vestnesa Ridge (~1,200 m water depth) and the 2) Storfjordenna gas hydrate mound in shallower waters (~380 m water depth; **Table 1**; **Figure 1**) (Bünz et al., 2012; Panieri et al., 2017; Serov et al., 2017). Macroscopic images of the studied carbonates are shown in **Figure 2**. We studied the carbonate geochemistry to elucidate the history of hydrocarbon seepage at these systems and to reveal potential factors influencing the fluid discharge for the different settings in the past. We used carbonate-C and -O isotope ratio measurements to constrain the carbon sources and to assess the possible influence of seawater and/or fluid from gas hydrates during carbonate precipitation. Seep carbonate-associated lipid biomarkers were analyzed to determine the microbial communities that were present at the time of carbonate precipitation. In this context, one of the prime objectives was to compare the isotope- and lipid biomarker-geochemical imprint of carbonates formed at the seafloor vs. those formed in deeper sediments, in order to find potential links between carbonate formation, methanotrophic communities and differential methane-seepage activity.

STUDY AREA

Vestnesa Ridge (~1,200 m water depth) is a NW-SE trending sediment drift off NW Svalbard. The eastern ridge segment is characterized by numerous pockmarks actively releasing methane

TABLE 1 | List of studied seep carbonates, sample locations, and remarks describing the samples and where they were collected.

Name	Sample ID	Location	Water depth (m)	Coordinates	Remarks
S-1	HH1029	Storfjordrenna	378	76.1069°N 15.9679°E	ROV-sampled seabed crust
S-2	HH1077	Storfjordrenna	378	76.1070°N 15.9694°E	ROV-sampled seabed crust
S-3	1520GC	Storfjordrenna	380	76.1,057°N 15.9661°E	Weakly lithified carbonate nodules, sampled with a gravity core at depth of 282 cmbsf
V-1	P1606002	Vestnesa Ridge	1,204	79.0026°N 69213°E	ROV-sampled seabed crust (P002 in **Figure 1**)
V-2	P1606011	Vestnesa Ridge	1,207	79.0076°N 6.8993°E	ROV-sampled seabed crust (P011 in **Figure 1**)
V-3	P1606012	Vestnesa Ridge	1,207	79.0077°N 68992°E	ROV-sampled seabed crust (P012 in **Figure 1**)
V-4	GeoB21616-1-2R-1E	Vestnesa Ridge	1,210	79.0069°N 69041°E	Cored crust sampled from MeBo core 127 at sediment depth of ~590–595 cmbsf (MeBo 127 in **Figure 1**)

GC, gravity core; ROV, remotely operated underwater vehicle; cmbsf, centimetres below seafloor.

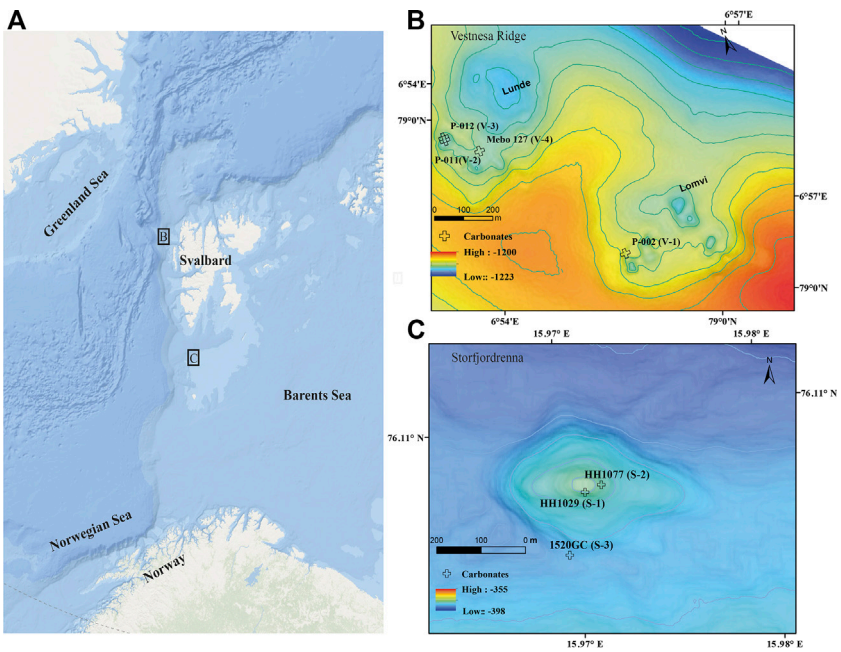

FIGURE 1 | (A) Overview of sampling locations at Vestnesa Ridge off NW Svalbard, and Storfjordrenna gas hydrate mound in the NW Barents Sea (Arctic base map from ArcGIS). **(B,C)** Detailed bathymetry maps and respective seep carbonate sample locations.

of a mixed microbial/thermogenic origin from the seafloor (e.g., Panieri et al., 2017; Pape et al., 2020). Previous investigations showed that the pockmarks cluster along sub-vertical faults (Plaza-Faverola et al., 2015). These investigations also suggest that seepage has likely been ongoing since the early Pleistocene (Knies et al., 2018).

Storfjordrenna is a trough-mouth fan south of Svalbard, NW Barents Sea, and the bathymetry (~380 m water depth) was highly influenced by the repeated growth and retreat of grounding glaciers. In contrast to Vestnesa Ridge, Storfjordenna was affected directly by the pressure release after the retreat of the grounded Scandinavian Ice Sheet during the last deglaciation, causing the destabilization of gas hydrate, which in turn led to the formation of seabed gas hydrate mounds, so-called gas hydrate pingos, that are up to 500 m in diameter and 10 m in height (Serov et al., 2017). Methane release from several seafloor mounds was observed previously, and shallow gas hydrates were recovered from several mounds, including the one studied here. The gas hydrate system of Storfjordrenna probably has existed since ~30,000 years BP (Serov et al., 2017), and comprises both active and inactive mounds, reflecting the spatio-temporal heterogeneity with regards to

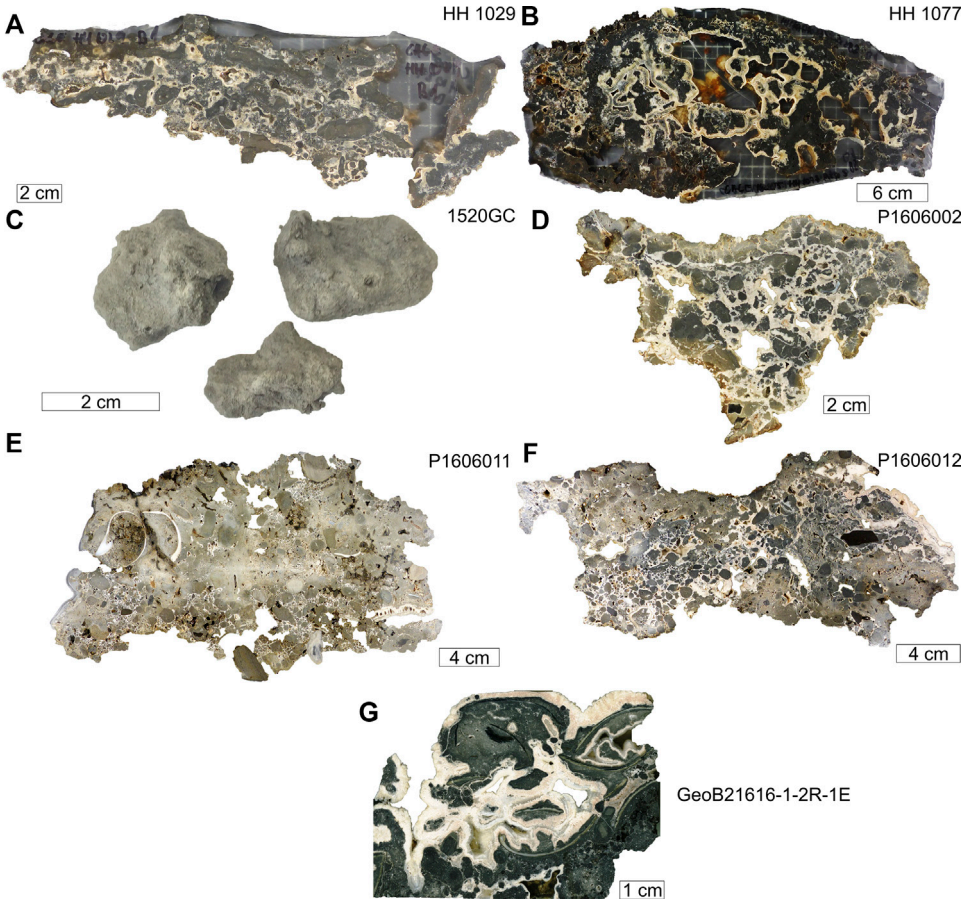

FIGURE 2 | Macroscopic photographs of the investigated seep carbonates [**(A–C)**: Storfjordrenna gas hydrate mound; **(D–G)**: Vestnesa Ridge)]; samples **(A,B,D–G)** are epoxy-impregnated cut slabs. **(A,B,D–G)** Porous intraformational breccias composed of rounded, dark gray microcrystalline aragonite cemented sediment clasts cemented by mm-to cm-thick whitish void-filling aragonite (adapted from Himmler et al., 2019). **(C)** Light gray microcrystalline Mg-calcite cemented sediment nodules. **(E–G)** with sporadic pebble-sized glaciogenic debris and bioclasts (gastropod and bivalve shell fragments).

methane transport and fluid seepage (Hong et al., 2017; 2018; Sen et al., 2018a; Yao et al., 2020).

MATERIALS AND METHODS

Sample Collection

At Vestnesa Ridge, seafloor samples (V-1, V-2, and V-3) were collected with the ROV Ægir 6000 during the R/V *G.O. Sars* cruise P1606 in 2016. The core sample (V-4) was retrieved during the cruise with R/V *Maria S. Merian*, expedition MSM 57, with the deep-sea drill rig MARUM-MeBo 70 in 2016. The carbonate specimen analyzed here was recovered from core MeBo 127 (V-4) at a sediment depth of ~ 5 m (Himmler et al., 2019). At the Strofjordrenna mound, seep carbonates were sampled from the seafloor (S-1 and S-2, **Table 1**) using the ROV by NTNU AMOS (Norwegian University of Science and Technology, Centre for Autonomous Marine Operations and Systems), and from the subsurface, using gravity coring (S-3) during expedition CAGE 16-5 on board of R/V *Helmer Hanssen* in 2016.

Carbonate Carbon and Oxygen Isotopes

Subsamples for stable carbon and oxygen isotope ratio analyses of samples S1, S2, and V1-V3 were obtained from freshly cut surfaces with a hand-held microdrill. Carbonate powders were treated at 70°C with anhydrous phosphoric acid in a GasBench II preparation line connected to a Thermo Scientific Delta V Advantage isotope ratio mass spectrometer (Thermo Fisher Scientific) at the Tallinn University of Technology (TUT), Estonia (Himmler et al., 2019). For stable carbon and oxygen isotopes of samples S-3 and V-4, subsamples were pulverized using an agate mortar, and the sample powders were placed in Thermo Scientific vials and flushed with helium gas. Afterward, five drops of anhydrous phosphoric acid were added manually. After equilibration (>3 h at 50°C), the liberated gas was analyzed on a Gasbench II and MAT253 Isotope Ratio Mass Spectrometer at UiT.

The $\delta^{13}C$ and $\delta^{18}O$ values are reported in per mill (‰) relative to the Vienna Pee Dee Belemnite (VPDB) standard. Normalization to the VPDB for carbon and oxygen isotope ratios was done using in-house standards. Analytical precision was estimated based on replicate measurements of samples and

standards (e.g., NBS-19, NBS-18), and was better than 0.1‰ for $\delta^{13}C$ and $\delta^{18}O$ analyses with the MAT253 IRMS and better than 0.2‰ for analyses of drilled samples with the Delta V Advantage.

Theoretical $\delta^{18}O$-fluid values were calculated using the fractionation factor-temperature relationship after Kim et al. (2007) (**Eq. 2**), and Grossman and Ku (1986) (**Eq. 3**), assuming O-isotope equilibrium with the ambient water during carbonate formation:

$$1000 \ln a_{aragonite-water} = 17.88 \times \frac{103}{T\,(Kelvin)} - 31.14 \quad (2)$$

$$\delta^{18}O_{water}\ (SMOW) = \delta^{18}O_{aragonite}\ (PDB) - \frac{19.7 - t\ (℃)}{4.34} \quad (3)$$

Mineralogy and Petrography

Mineralogical compositions were determined by X-ray diffraction (XRD) on homogenized bulk-rock powders. All samples were analyzed on a Bruker D8 Advance X-ray diffractometer (Cu Kα radiation in 3–75° 2θ range; Sauer et al., 2017). Quantitative data were obtained with the Rietveld algorithm-based code, Topas-5, provided by Bruker. A displacement correction of the spectrum was applied relative to the main quartz peak, and the Mg content in calcite was quantified based the single peak displacement (calcite d_{104}) in the diffraction pattern to estimate the amount of $MgCO_3$ mol% (mole percentage vs. the total carbonate content) in the analyzed samples (Goldsmith et al., 1958).

Petrographic thin sections (~30 μm thick; 6.5 cm × 5 cm) of ROV-sampled and the cored seep carbonate crust samples were prepared from epoxy-fixed cut slabs. Thin sections have been examined with transmitted polarized light microscopy using a Zeiss Axioplan2 equipped with an AxioCam ERc 5s digital camera. Single images were stitched together using the tiles tool of the Zeiss ZEN blue software.

Lipid Biomarkers

Seep carbonates were crushed into centimetre-sized chips and thoroughly washed with deionized (DI) water. Similarly, loose sediment was removed from the weakly lithified carbonate nodules by washing with DI. The cleaned chips and nodules were placed with sanitized stainless-steel tweezers into a glass beaker before slowly adding 37% HCl to dissolve the carbonate matrix (Niemann et al., 2005). The resulting solution was extracted with organic solvents, and lipids were analyzed according to previously reported protocols (Elvert et al., 2003) with modification for alcohol derivatization and instrument setup (Niemann et al., 2005; Blees et al., 2014). Briefly, a total lipid extract (TLE) was obtained by four-step solvent extraction with decreasing polarity of the carbonate solution: dichloromethane (DCM)/methanol (MeOH) 1:2; DCM/MeOH 2:1; and two times DCM. The TLE was then saponified with 12% KOH in MeOH for 3 h at 80°C. A neutral fraction was extracted with hexane before methylation with BF_3/MeOH of the fatty acids, yielding fatty acid methyl esters (FAMEs) for gas-chromatographic (GC) analysis. Concentrations of the different fractions were examined using a GC (Thermo Scientific TRACETM Ultra, Rxi-5ms column) with flame ionization detection (FID). Identification of individual compounds after GC was achieved by quadrupole mass spectrometry (GC-MS) (Thermo Scientific DSQ II). Compound-specific stable carbon isotope ratios were determined using an isotope ratio mass spectrometry (IRMS) unit (Thermo Scientific Delta V Advantage) coupled to a GC setup with the same specification as outlined above. Concentrations and stable carbon isotope ratios were calibrated/normalized using internal standards. Compounds specific stable carbon isotope compositions are reported as $\delta^{13}C$ in ‰ relative to VPDB, and have an analytical error of less than ±1.5‰.

RESULTS

Carbonate Mineralogy, Petrography and Stable Carbon and Oxygen Isotopes

Aragonite and magnesium calcite dominated the carbonate mineralogy of the seafloor samples from both Storfjordrenna (S1-S2) and Vestnesa Ridge (V1-V3). The in-core sample from Storfjordrenna (S-3) was comprised mainly of high-Mg-calcite, whereas the MeBo core sample (V-4) from 590 to 595 cmbsf was mostly aragonitic. Quartz and plagioclase were the main non-carbonate minerals in the samples (**Table 2**).

The seabed-sampled carbonate crusts comprised porous intraformational breccias of microcrystalline carbonate-cemented sediment clasts. Cement consists of mm-to cm-thick aragonite (**Figure 2**). Carbonates sampled from the shallow subsurface (S-3) comprised gray Mg-calcite-cemented, irregular shaped nodules (~2 cm in diameter; **Figure 2**). Clotted and peloidal fabrics, as well as cemented tubes of siboglinid tube worms are common in the Storfjordrenna crusts (**Figures 3A**,**B**; Sen et al., 2018b). The carbonates contained a few mollusc-shell fragments (bivalves and gastropods) (**Figure 3C-F**). The carbonate-cemented sediment clasts of the breccias contained abundant silt to fine-sand sized siliciclastic grains, mostly quartz and feldspar. Fine grained cryptocrystalline aragonite was abundant in the cored sample (V-4), enclosing microcrystalline aragonite-cemented sediment.

The carbonate $\delta^{13}C$ values ranged from −36 to −20‰, and the $\delta^{18}O$ values from 4 to 7‰ (**Figure 4**). The dashed lines in **Figure 4** represent the calculated theoretical $\delta^{18}O$ of aragonite formed in isotopic equilibrium with sea water according to **Eqs. 2** and **3** (aragonite-1 and -2), respectively, and assuming ambient seawater temperatures (−1.5 and 1.9°C) and $\delta^{18}O$ (0‰) at the two study sites. The $\delta^{18}O$ values of the investigated seep carbonates were all above the calculated values for aragonite-1 and -2.

Lipid Biomarker Inventory

Lipid contents and compound-specific $\delta^{13}C$ values are listed in **Table 3**. In the fatty-acid fraction of all samples, we found iso- and anteiso-C15:0 fatty acids with low $\delta^{13}C$-values in the range of −60 to −100‰. Similarly, the isoprenoid glycerol diethers archaeol and *sn2*-hydroxyarchaeol were detected in the alcohol fractions of all samples with $\delta^{13}C$-values of −83 to −109‰. The irregular isoprenoid hydrocarbon crocetane was not detectable in

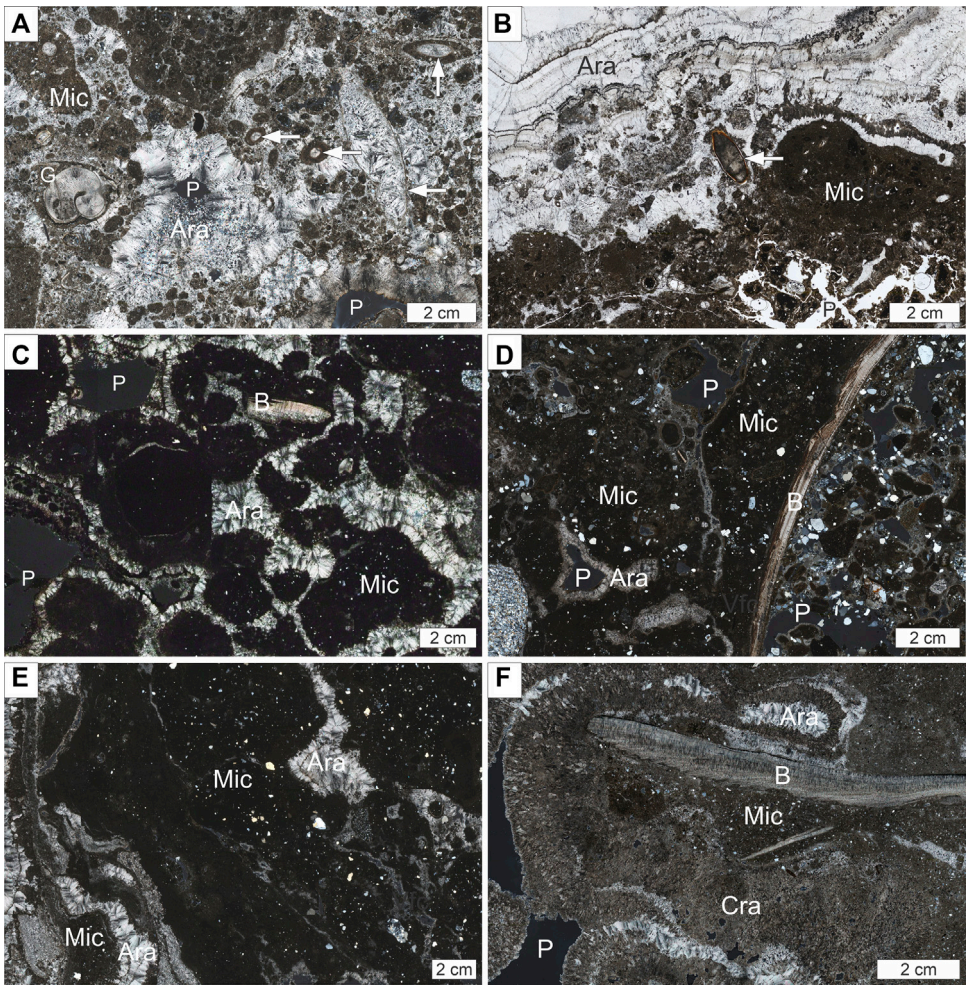

FIGURE 3 | Representative photomicrographs (stitched tiles) of the seep carbonate crusts. **(A)** Microcrystalline aragonite-cemented sediment (Mic) clasts with abundant silt-sized quartz, gastropod fragment(G), and abundant clotted micrite clasts and peloids cemented by botryoidal and fibrous aragonite (*Ara*); arrows point to cemented tube worm tubes; cross-polarized light, pore space (P) appears dark [sample HH 1029 (S-1)] **(B)** Porous (P) microcrystalline aragonite-cemented sediment (Mic) with abundant silt-sized quartz (lower image half) and cm-thick aragonite cement (*Ara*) with abundant clotted micrite inclusions and multiple thin dark bandings; arrow points to tube worm [parallel-polarized light, pore space appears bright; HH 1077(S-2)]. **(C)** Microcrystalline aragonite-cemented sediment (Mic) clasts with abundant silt-sized quartz cemented by botryoidal aragonite (*Ara*); note a bivalve shell fragment (B); cross-polarized light, pore space (P) appears dark [P1606002(V-1)]. **(D)** Microcrystalline aragonite-cemented sediment (Mic) with abundant silt to fine sand sized quartz; not quartzite pebble (lower left) and bivalve shell (B); pores and fractures are lined with botryoidal and fibrous aragonite (*Ara*); cross-polarized light, pore space (P) appears dark [P1606011(V-2)]. **(E)** Microcrystalline aragonite-cemented sediment (Mic) with abundant silt-sized quartz and fracture-filling botryoidal aragonite (*Ara*); cross-polarized light [P1606012(V-3)]. **(F)** Microcrystalline aragonite cemented sediment (Mic) with abundant silt-sized quartz and bivalve fragment (B) surrounded by cryptocrystalline aragonite (Cra) and botryoidal aragonite (*Ara*); cross-polarized light, pore space (P) appears dark [GeoB21616-1-2R-1 E (V-4)]. **(C–F)** adapted from Himmler et al. (2019).

the cored nodule carbonate from Storfjordrenna 1520GC (S-3), and we only found minor amounts in the seafloor crust from Vestnesa (V-3). The irregular isoprenoid hydrocarbon 2,6,10,15,19-pentamethyleicosane (PMI) was present in all samples, but concentrations in V-1 and V-2 were low (0.05 and 0.03 μg/g carbonate). The δ^{13}C-values of the isoprenoid hydrocarbons were always below −91‰.

Typical MOx-related lipids such as a 4α-methyl sterol and diplotene were also present in all samples, with δ^{13}C values of about −50‰. We found substantially lower isotope signatures in these compounds only in the Vestnesa core carbonate (V-4; 4α-methyl sterol: −108‰, Diploptene: −79‰).

DISCUSSION

Lipid Biomarker Constrains on Microbial Communities During Carbonate Precipitation

AOM Communities

At cold seeps, a substantial fraction of the uprising methane is consumed in sediments by anaerobic methane-oxidizing archaea (ANME-1, -2, -3), often in association with sulfate-reducing partner bacteria of the DSS and DSB clade (Knittel and Boetius, 2009; Milucka et al., 2012; Wegener et al., 2015;

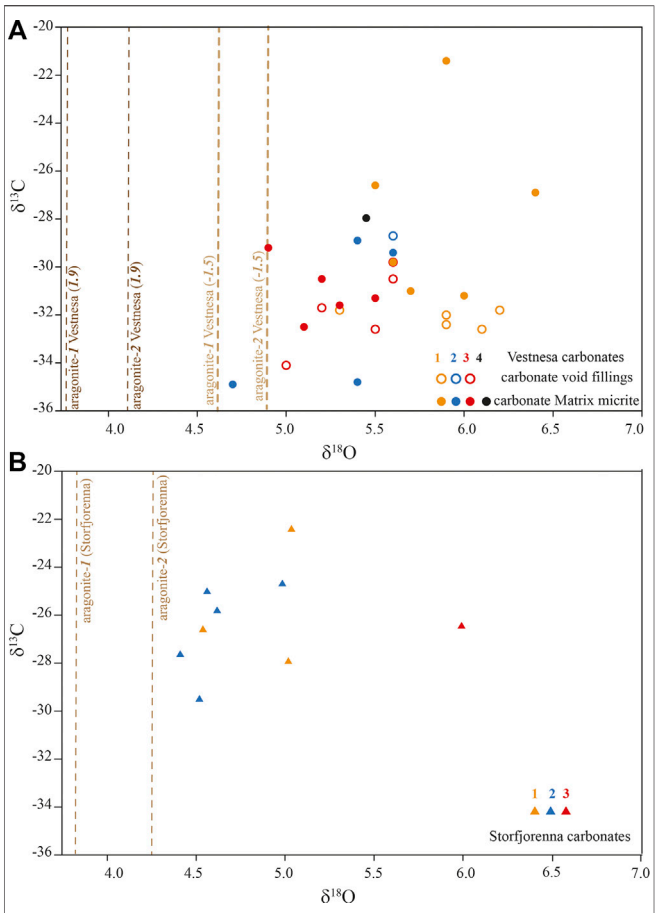

FIGURE 4 | Carbonate stable carbon and oxygen isotope compositions in **(A)**. Vestnesa Ridge and **(B)** Storfjordrenna. The dashed lines indicate the theoretical $\delta^{18}O$ values of aragonite-1 (Kim et al., 2007), aragonite-2 (Grossman and Ku, 1986) expected for precipitation in equilibrium with bottom water temperature, according to **Eqs. 2** and **3**, respectively. For Vestnesa, two different temperatures were assumed based on the reconstructed temperature from foraminifera (Dessandier et al., 2019).

Gründger et al., 2019). Methane bypassing the AOM filter and reaching oxic sediments at the seafloor or the water column then can be consumed by methanotrophic bacteria (MOB) which mediate the aerobic oxidation of methane (MOx; Niemann et al., 2006; Reeburgh, 2007; Steinle et al., 2015). Specific lipid biomarkers can be used to identify the dominant microbes involved in AOM and MOx (Elvert and Niemann, 2008; Niemann and Elvert, 2008), and to differentiate between the two main modes of methane oxidation. Lipids of (methanotrophic) microbes are encased in the carbonate matrix at the time of mineral precipitation. Lipids can hence be used to assess the biogeochemical environment. (Blumenberg et al., 2004; Niemann and Elvert, 2008; Birgel et al., 2011; Himmler et al., 2015).

Diagnostic archaeal and bacterial lipids detected here were strongly depleted in ^{13}C, providing conclusive evidence for the occurrence of microbial communities performing AOM (Niemann and Elvert, 2008), as well as MOx (Elvert and Niemann, 2008). Overall, the lipid biomarker inventory characterized by low *sn2*-hydroxyarchaeol/archaeol ratios <0.3 and an aiC15:0/iC15:0 FA ratio of 0.1–1.2 was similar to carbonates from other seep sites, including the Congo Fan (Feng et al., 2010), the Gulf of Mexico (Birgel et al., 2011; Feng et al., 2014), and the South China Sea (Guan et al., 2016). In contrast, quite different ANME- and SRB-related lipids were found at other seep sites (e.g., with a much higher *sn2*-hydroxyarchaeol/archaeol ratio $\gg 1$; Niemann et al., 2005; Niemann et al., 2006; Guan et al., 2019). This difference in lipid contents is most likely related to different types of microorganisms that become encased in the carbonate precipitates (Niemann and Elvert, 2008).

Indeed, ANME-1/DSS, ANME-2/DSS, and ANME-3/DBB consortia can be distinguished based on their lipid biomarker and isotopic fingerprints (Niemann and Elvert, 2008). For example, ANME-2/DSS consortia are characterized by the presence of crocetane, while PMIs with four and five double bonds without any higher saturated homologs were only found in ANME-3. Both ANME-2 and -3 are characterized by an elevated (typically >1.1) *sn2*-hydroxyarchaeol (OH-ar) to archaeol (OH-ar/ar) ratio, which distinguishes them from ANME-1/DSS (Niemann and Elvert, 2008). Accordingly, the low OH-ar/ar ratios of 0.1–0.3 (**Table 3**) suggest the presence of ANME-1/DSS. However, we also observed high concentrations of crocetane in all carbonates except for S-3 and V-3. Crocetane is abundant in ANME-2, but is typically only found in minor amounts, or not at all, in ANME-1 (Niemann and Elvert, 2008 and reference therein). Its absence, while not conclusively diagnostic, is consistent with an ANME-1/DSS dominated seep environments (Haas et al., 2010). ANME-1 microbes at some ancient seeps have been identified in a similar manner (Peckmann et al., 2009; Natalicchio et al., 2015). We argue that the lower stability of *sn2*-hydroxyarchaeol can explain our finding of low OH-ar/ar ratios (in the presence of elevated crocetane concentrations), i.e., *sn2*-hydroxyarchaeol loses its hydroxyl group during (early) diagenesis so that the *sn2*-hydroxyarchaeol to archaeol ratio decreases. Furthermore, the saturated hydrocarbon crocetane is probably more stable, such that its presence in our carbonate samples indicates that the AOM community at the time of precipitation was either ANME-2 dominated or comprising a mixture of ANME-2 and ANME-1. Only carbonate S-3 did not contain detectable amounts of crocetane, pointing to ANME-1 as the dominant AOM microbes in this sample. Carbonate sample S-3 also contained a higher proportion of Mg-calcite, suggesting a lower methane flux at the time of precipitation (see *Discussion* in the following section). This is also consistent with a prevalence of ANME-1, which often dominates low methane flux sites (Knittel et al., 2005; Gründger et al., 2019). It was shown previously that the dominant microbial community in relatively deep sediments (70 cmbsf) at the Storfjordrenna seeps was ANME-1/Seep-SRB1 (Gründger et al., 2019), which is consistent with the lipid biomarker signature of the Mg-calcite dominated nodular seep carbonate (S3) recovered from 282 cmbsf. However, we also found signatures typical for MOx communities in this carbonate (see section *MOx-Communities* below), which raises the question of

TABLE 2 | Mineralogical compositions (weight-%) of the carbonates.

Name	Sample ID	Aragonite	Mg-calcite	Dolomite	Quartz	Plagioclase
S-1	HH1029	55	23		10	3
S-2	HH1077	75	10		7	2
S-3	1520GC		60	1	23	4
V-1	P1606002	61	11	Trace	12	5
V-2	P1606011	40	2		23	11
V-3	P1606012	70				
V-4	MeBo 127	77	2		10	4

Mg-calcite, magnesium-calcite.

whether the carbonate was indeed precipitated in deep anoxic sediments.

^{13}C-depleted, terminally branched ai-C15:0 and i-C15:0 fatty acids are diagnostic biomarkers for SR partner bacteria (Niemann and Elvert, 2008). The ratio of ai-C15:0/i-C15:0 of ~1 in all samples points to ANME-2 associated SEEP-SRB1 or *Desulfobulbus* associated to ANME-3. However, we could not find the fatty acid cyC17:0ω5,6, which is typically indicative of the ANME-2 associated SRB, nor-C17:1ω6 which is diagnostic for the ANME-3 partner SRB (Niemann and Elvert, 2008 and reference therein). Nevertheless, with respect to the probable prevalence of ANME-2 in the studied systems (except sample S3), we suggest that the fatty acid pattern is rather indicative of the ANME-2 associated SEEP-SRB1.

MOx-Communities

The seep carbonates contained high abundances of ^{13}C-depleted diplotene and 4α-methyl sterol (compound Ib in Elvert and Niemann, 2008), respectively, which were suggested as characteristic markers for Type I MOB (Elvert and Niemann, 2008). MOx is a strictly aerobic process usually occuring at the seafloor or in the water column, where both dissolved oxygen and methane are available. To the best of our knowledge, only a few indications exists from fresh water environments that some MOB-type microbes can use alternative electron acceptors such as nitrate or sulfate (van Grinsven et al., 2020a; van Grinsven et al., 2020b). But the environmental significance of these modes of methane oxidation, in particular in marine systems, is unclear. Both, the seafloor and core samples at Vestnesa Ridge (V1–V4) contained diplotene and the 4α-methyl sterol with a substantial to moderate ^{13}C-depletion (−108 to −45‰), similar to what has been observed in some of the modern seep carbonates (Birgel et al., 2011; Himmler et al., 2015; Guan et al., 2016) and in surface sediments of active cold seeps (Elvert and Niemann, 2008). Following those findings, we propose that their presence in seep carbonates indicates less reducing, or intermittent microaerophilic, conditions during carbonate precipitation (Birgel et al., 2011). The co-encasing of both AOM and MOx-derived lipids strongly suggests that the spatial distance between AOM and MOx zones must have been very small. Such conditions are typically found in present-day systems where the methane flux rates are very high, preventing sulfate from penetrating deeper into the seafloor and thus limiting AOM to the sediment surface (Niemann et al., 2006; Lösekann et al., 2007; Lee et al., 2019). We argue that the co-occurrence of AOM- and MOB-derived lipids furthermore demonstrates that, at the time of carbonate precipitation, the system must have vented vigorously, releasing substantial amounts of methane into the water column. Sedimentary MOx communities typically occur when methane bypasses the AOM filter in deeper sediments (Niemann et al., 2006; Birgel et al., 2011; Steinle et al., 2016). MOx alone is typically less effective compared to AOM with regards to preventing methane emissions from the seafloor because MOx demands oxygen, which restricts MOx communities often to a thin layer at the sediment surface. Hence, sedimentary MOx can only retain a rather limited fraction of benthic methane, in particular when the overall methane flux is high. In contrast, in systems characterized by low methane fluxes, methane is typically consumed in deeper sediment layers, within a well-defined SMTZ (Knittel and Boetius, 2009), so that MOB communities generally do not develop at the sediment surface. Thus, we interpret our biomarker-based finding that both aerobic and anaerobic methanotrophs were encapsulated in the same carbonate matrix reflecting past periods of high methane flux. These high-flux periods could have also been related to a non-steady state of methane flux with a not fully-developed AOM community, or episodic pulses of high methane fluxes that bypass the AOM barrier and reach oxic surface sediments (Yao et al., 2019).

Our biomarker findings are also consistent with the mineralogical composition of the carbonate samples. Highest hopanoid contents were found in the aragonite-dominated core carbonate in Vestnesa (V-4), with ANME-2/DSS most likely as the dominant consortia. Together, the geochemical and mineralogical evidence suggest that carbonates retrieved from the sediment cores in Vestnesa were precipitated very close to the seafloor (Himmler et al., 2019), i.e., a favourable environment for MOx. Nevertheless, at this point, we cannot sufficiently explain the presence of MOB-diagnostic hopanoids in sample S-3 from Storfjordrenna. All evidence (other than the presence of isotopically depleted MOB lipids in the carbonate), point to the S-3 carbonate precipitation in deeper sediment layers, and a persistent anoxic environment that would not support MOB community development. Possibly, the Mg-calcite dominated carbonate nodule precipitated in reduced sediments that were still close enough to the redox-transition zone to also encase MOx-related lipids. Alternatively, it may have formed in deeper sediments, and subsequently exposed to a more oxic environment and overprinted by a second layer of MOB-derived lipids before burial in deeper sediments.

Carbonate δ^{13}C and δ^{18}O Indicate Gas Hydrate Dissociation During Precipitation

Sampled carbonates from the seabed and core samples from both Storfjordrenna and Vestnesa display very negative δ^{13}C values (**Figure 2**). The observed δ^{13}C values (−36 to −20‰) fall into the typical δ^{13}C range for methane seep carbonates (Lein, 2004; Naehr et al., 2007). Seep-carbonate δ^{13}C reflects a mixture of different carbon sources including dissolved inorganic carbon (DIC) from seawater, oxidized organic matter, and residual DIC

TABLE 3 | Lipid biomarker concentrations and compound-specific $\delta^{13}C$ values.

	HH 1029 (S-1)		HH 1077 (S-2)		1520 GC (S-3)		P1606002 (V-1)		P1606011 (V-2)		P1606012 (V-3)		MeBo 127 (V-4)	
	Concentration (µg/g carbonate)	$\delta^{13}C$ (‰)	Concentration (µg/g carbonate)	$\delta^{13}C$ (‰)	Concentration (µg/g carbonate)	$\delta^{13}C$ (‰)	Concentration (µg/g carbonate)	$\delta^{13}C$ (‰)	Concentration (µg/g carbonate)	$\delta^{13}C$ (‰)	Concentration (µg/g carbonate)	$\delta^{13}C$ (‰)	Concentration (µg/g carbonate)	$\delta^{13}C$ (‰)
I-15-FA	0.30	−62	0.31	−76	0.42	−39	0.85	−74	0.40	−83	2.79	−91	0.76	−99
Ai-15-FA	0.35	−64	0.45	−76	0.34	−33	0.85	−71	0.40	−70	0.35	−78	0.87	−90
Ar	1.00	−102	3.64	−99	0.49	−90	0.71	−99	0.67	−104	0.82	−105	11.37	−109
OH-Ar	0.16	−95	0.94	−101	0.07	−93	0.13	n.d.	0.13	−103	0.27	−105	0.49	−83
4α methyl sterol	0.04	−45	0.14	−57	0.29	−64	0.02	−52	0.03	−46	0.02	−61	0.16	−108
Diploptene	0.08	−54	0.36	−52	0.15	−46	0.17	−51	0.18	−52	0.15	n.d.	0.70	−79
crocetane	0.36	−97	1.65	−105	n.d.	n.d.	0.30	−99	0.47	−103	0.05	n.d.	1.76	−115
PMI:0	0.07	−91	0.20	−96	0.09		0.03		0.05	−100	0.03	n.d.	0.14	−113
OH-Ar/Ar	0.2		0.3		0.1		0.2		0.2		0.3		0.04	
Ai-15-FA/I-15-FA	1.2		1.4		0.8		0.9		1.0		0.1		1.1	
$\Delta\delta^{13}C$ Ar-OH-Ar	−6		3		3				−1				−27	

FA, fatty acids; PMI, pentamethyleicosane; Ar, archaeol; OH-Ar, sn2-hydroxylarchaeol; n. d, not determined, content too low for accurate analysis.

affected by methanogenesis in addition to DIC derived from AOM (e.g., Peckmann and Thiel, 2004). AOM produces very low-$\delta^{13}C$ DIC carbon isotope signatures because the organisms preferentially utilize an already ^{13}C-depleted carbon source (i.e., methane) for biomass production, and additionally discriminate against ^{13}C during methane oxidation (Whiticar, 1999; Holler et al., 2009). The methane source at both sampling locations represents a mixture of thermogenic and microbial origins, with $\delta^{13}C$ values of −48‰ at Storfjordrenna (Serov et al., 2017), and −54‰ at Vestnesa (Panieri et al., 2017), respectively. Porewater DIC $\delta^{13}C$ at Storfjordrenna is about −28‰, and −32‰ at Vestnesa Ridge. The average $\delta^{13}C$ value of organic carbon from the investigated Storfjordrenna gas hydrate mound is −26‰ (**Supplementary Table S1**), and around −25‰ (Sauer et al., 2020) at Vestnesa. Mineralization of organic carbon produces DIC with almost the same carbon isotope composition (Presley and Kaplan, 1968). Given that the observed carbonate $\delta^{13}C$ values (−36 to −20‰) best match the pore water DIC $\delta^{13}C$ values, and are generally lower than those expected for DIC produced from organic matter remineralization, we conclude that the carbonates have incorporated a higher portion of methane-derived porewater DIC, compared to carbon from sedimentary organic matter or seawater-derived carbon.

Information on the oxygen isotopic composition of the fluid (from which the carbonates precipitated) can be deduced from seep carbonate $\delta^{18}O$-values (e.g., Greinert et al., 2001; Naehr et al., 2007). In turn, the ^{18}O-signature of the ambient water can be used to constrain the environmental setting of carbonate precipitation. Assuming that aragonite formed in isotopic equilibrium with bottom water at temperatures that are similar to those today, and assuming a $\delta^{18}O$-value of 0‰ (V-SMOW) for the seawater, the theoretical $\delta^{18}O$ aragonite values would be 3.8 (**Eq. 2**) – 4.3‰ (**Eq. 3**) in Storfjordrenna, and 3.8 (**Eq. 2**)–4.9‰ (**Eq. 3**) at Vestnesa Ridge. Remarkably, the measured carbonate $\delta^{18}O$-values are substantially higher than these calculated equilibrium values (**Figure 4**). The higher $\delta^{18}O$ values of the authigenic carbonates suggest the incorporation of O-atoms from an ^{18}O-enriched fluid during carbonate precipitation. Such ^{18}O-enriched fluid might originate from gas hydrate dissociation (Hesse and Harrison, 1981; Ussler and Paull, 1995), clay mineral dehydration (Hesse, 2003), or deep-sourced fluids modified by mineral-water interactions (Giggenbach, 1992). The lipid and mineralogy data suggest that most of our samples (except S-3) were formed close to the seafloor, yet the observed carbonate $\delta^{18}O$ values clearly do not support O incorporation from average seawater and suggest that O-isotope exchange with ^{18}O-rich fluids overprinted the seawater $\delta^{18}O$-signal of about 0‰. Discerning a fluid source (e.g., gas hydrate vs. mineral dewatering) based on the carbonate $\delta^{18}O$ values alone is ambiguous. Yet, considering that gas hydrates are present in shallow sediments at both sampling sites (Panieri et al., 2017; Serov et al., 2017), it seems reasonable that at least some of the ^{18}O-enrichment of the carbonate can be attributed to O-atom incorporation from fluids derived from gas hydrate dissociation (Greinert et al.,

2001; Naehr et al., 2007), as assumed from ^{18}O-enrichment in foraminifera shells in the same region (Dessandier et al., 2019).

Seep Carbonate Mineralogy

All carbonates recovered from Vestnesa Ridge (at the seafloor and in the core; V1–V4) as well as Storfjordrenna carbonates S1 and S2 are predominantly composed of aragonite, whereas the nodular carbonate from Storfjordrenna (S-3) was mostly Mg-calcite. This difference in seep carbonate mineralogy has been observed previously (Bohrmann et al., 1998; Crémière et al., 2016b), and was attributed to the formation environment (Burton, 1993; Mazzini et al., 2004). At seeps, carbonate precipitation occurs when the fluids become oversaturated with AOM-produced bicarbonate and if the required dissolved cations (i.e., Ca^{2+}, Sr^{2+}, Mg^{2+}) are available. More precisely, formation of aragonite is favored over Mg-calcite at high-sulfate and low-sulfide concentrations (Burton, 1993; Bayon et al., 2007). Therefore, aragonite-dominated seep carbonates are expected to form closer to the seafloor because of the higher sulfate concentration in seawater, as sulfate is generally depleted in deeper sediments (Bohrmann et al., 1998; Aloisi et al., 2000; Feng et al., 2014; Crémière et al., 2016b). Precipitation of aragonite at the seafloor is consistent with our findings of co-occuring AOM and MOx-derived lipids in the carbonates, which also indicate precipitation close the sea floor. The Mg-calcite rich sample from Storfjordrenna, on the other hand, indicates a formation at a relatively low methane flux in deeper sediments.

SUMMARY AND CONCLUSION

In this study, seep-carbonate samples from two active Arctic gas hydrate sites, Vestnesa Ridge and Storfjordrenna gas hydrate mounds, were investigated. The carbonate carbon and oxygen isotope ratios, carbonate mineralogy, and lipid biomarker inventories indicate where, and under which environmental conditions, the carbonates were formed originally. The ^{13}C-depleted carbon and ^{18}O-enriched isotope signatures of all carbonates reflect methane carbon incorporation (via AOM), and a precipitation environment where carbonates are formed in isotopic equilibrium with porewater affected by gas hydrate dissociation. ^{13}C-depleted biomarkers in all samples reveal the presence of ANME-2/DSS microbial consortia at the time of carbonate precipitation and their entombment in the authigenic carbonate matrix. Furthermore, the recovery of lipids in the mostly aragonitic carbonates, which typically originate from aerobic methanotrophs, indicates the close proximity of anoxic and oxic methane oxidation zones in the shallow sediments, implying high methane fluxes and probably methane ebullition to the water column at the time when the carbonates were precipitated. We suggest that the combined analysis of carbonate mineralogy and lipid biomarker contents in a geochronological context (e.g., through U/Th-dating of carbonates) has the potential to reconstruct the magnitude of seepage activity in the past.

DATA AVAILABILITY STATEMENT

The original contributions presented in the study are included in the article/**Supplementary Material**, further inquiries can be directed to the corresponding author.

AUTHOR CONTRIBUTIONS

HY collected the samples and performed the biomarker analysis under supervision with GP and HN. TH provided support for mineralogy and ML provided support for biomarker experiments. All authors contributed to the writing of the manuscript at all stages.

FUNDING

This work was supported by the Research Council of Norway through its Centre of Excellence funding scheme for CAGE, project number 223259, and partially by the NORCRUST project, grant number 255150.

ACKNOWLEDGMENTS

We thank Tõnu Martma from the Tallinn University of Technology for the stable isotope analyses, Jasmin Schoenenberger from NGU for the XRD analysis of carbonate samples, as well as the captain, crew members, and scientific team of R/V Helmer Hanssen, R/V G.O. Sars, R/V Maria S. Merian for their contribution during the research cruises CAGE16-5, P1606 and MSM57.

SUPPLEMENTARY MATERIAL

The Supplementary Material for this article can be found online at: https://www.frontiersin.org/articles/10.3389/feart.2020.570742/full#supplementary-material.

REFERENCES

Aloisi, G., Pierre, C., Rouchy, J.-M., Foucher, J.-P., and Woodside, J. (2000). Methane-related authigenic carbonates of Eastern Mediterranean Sea mud volcanoes and their possible relation to gas hydrate destabilisation. *Earth Planet Sci. Lett.* 184, 321–338. doi:10.1016/S0012-821X(00)00322-8

Argentino, C., Lugli, F., Cipriani, A., Conti, S., and Fontana, D. (2019). A deep fluid source of radiogenic Sr and highly dynamic seepage conditions recorded in Miocene seep carbonates of the northern Apennines (Italy). *Chem. Geol.* 522, 135–147. doi:10.1016/j.chemgeo.2019.05.029

Bayon, G., Pierre, C., Etoubleau, J., Voisset, M., Cauquil, E., Marsset, T., et al. (2007). Sr/Ca and Mg/Ca ratios in Niger Delta sediments: implications for authigenic carbonate genesis in cold seep environments. *Mar. Geol.* 241, 93–109. doi:10.1016/j.margeo.2007.03.007

Bintanja, R. (2018). The impact of Arctic warming on increased rainfall. *Sci. Rep.* 8, 16001. doi:10.1038/s41598-018-34450-3

Birgel, D., Feng, D., Roberts, H. H., and Peckmann, J. (2011). Changing redox conditions at cold seeps as revealed by authigenic carbonates from Alaminos Canyon, northern Gulf of Mexico. *Chem. Geol.* 285, 82–96. doi:10.1016/j.chemgeo.2011.03.004

Birgel, D., Himmler, T., Freiwald, A., and Peckmann, J. (2008). A new constraint on the antiquity of anaerobic oxidation of methane: late Pennsylvanian seep limestones from southern Namibia. *Geology* 36, 543. doi:10.1130/g24690a.1

Blees, J., Niemann, H., Wenk, C. B., Zopfi, J., Schubert, C. J., Jenzer, J. S., et al. (2014). Bacterial methanotrophs drive the formation of a seasonal anoxic benthic nepheloid layer in an alpine lake. *Limnol. Oceanogr.* 59, 1410–1420. doi:10.4319/lo.2014.59.4.141E

Blumenberg, M., Seifert, R., Reitner, J., Pape, T., and Michaelis, W. (2004). Membrane lipid patterns typify distinct anaerobic methanotrophic consortia. *Proc. Natl. Acad. Sci. U.S.A.* 101, 11111–11116. doi:10.1073/pnas.0401188101

Bohrmann, G., Greinert, J., Suess, E., and Torres, M. (1998). Authigenic carbonates from the Cascadia subduction zone and their relation to gas hydrate stability. *Geology*. Editor C. K. Paull and W. P. Dillon, 26, 647–650. doi:10.1130/0091-7613(1998)026<0647:acftcs>2.3.co;2

Bünz, S., Polyanov, S., Vadakkepuliyambatta, S., Consolaro, C., and Mienert, J. (2012). Active gas venting through hydrate-bearing sediments on the Vestnesa Ridge, offshore W-Svalbard. *Mar. Geol.* 332-334, 189–197. doi:10.1016/j.margeo.2012.09.012

Burton, E. A. (1993). Controls on marine carbonate cement mineralogy: review and reassessment. *Chem. Geol.* 105, 163–179. doi:10.1016/0009-2541(93)90124-2

IPCC, et al. (2013). "Climate change 2013: the physical science basis," in *Contribution of working group I to the fifth assessment report of the intergovernmental panel on climate change*. Editors T. F. Stocker, D. Qin, G.-K. Plattner, M. M. B. Tignor, S.K. Allen, J. Boschung, et al. (Cambridge, United Kingdom and New York, NY, USA:Cambridge University Press), 1535.

Crémière, A., Lepland, A., Chand, S., Sahy, D., Condon, D. J., Noble, S. R., et al. (2016a). Timescales of methane seepage on the Norwegian margin following collapse of the Scandinavian Ice Sheet. *Nat. Commun.* 7, 11509. doi:10.1038/ncomms11509

Crémière, A., Lepland, A., Chand, S., Sahy, D., Kirsimäe, K., Bau, M., et al. (2016b). Fluid source and methane-related diagenetic processes recorded in cold seep carbonates from the Alvheim channel, central North Sea. *Chem. Geol.* 432, 16–33. doi:10.1016/j.chemgeo.2016.03.019

Dessandier, P.-A., Borrelli, C., Yao, H., Sauer, S., Hong, W.-L., and Panieri, G. (2020). Foraminiferal δ18O reveals gas hydrate dissociation in Arctic and North Atlantic ocean sediments. *Geo Mar. Lett.* 40, 507–523. doi:10.1007/s00367-019-00635-6

Dickens, G. R. (2003). Rethinking the global carbon cycle with a large, dynamic and microbially mediated gas hydrate capacitor. *Earth Planet Sci. Lett.* 213, 169–183. doi:10.1016/s0012-821x(03)00325-x

Dickens, G. R., O'Neil, J. R., Rea, D. K., and Owen, R. M. (1995). Dissociation of oceanic methane hydrate as a cause of the carbon isotope excursion at the end of the Paleocene. *Paleoceanography* 10, 965–971. doi:10.1029/95pa02087

Elvert, M., Boetius, A., Knittel, K., and Jørgensen, B. B. (2003). Characterization of specific membrane fatty acids as chemotaxonomic markers for sulfate-reducing bacteria involved in anaerobic oxidation of methane. *Geomicrobiol J.* 20, 403–419. doi:10.1080/01490450303894

Elvert, M., and Niemann, H. (2008). Occurrence of unusual steroids and hopanoids derived from aerobic methanotrophs at an active marine mud volcano. *Org. Geochem.* 39, 167–177. doi:10.1016/j.orggeochem.2007.11.006

Feng, D., Birgel, D., Peckmann, J., Roberts, H. H., Joye, S. B., Sassen, R., et al. (2014). Time integrated variation of sources of fluids and seepage dynamics archived in authigenic carbonates from Gulf of Mexico Gas Hydrate Seafloor Observatory. *Chem. Geol.* 385, 129–139. doi:10.1016/j.chemgeo.2014.07.020

Feng, D., Chen, D., Peckmann, J., and Bohrmann, G. (2010). Authigenic carbonates from methane seeps of the northern Congo fan: microbial formation mechanism. *Mar. Petrol. Geol.* 27, 748–756. doi:10.1016/j.marpetgeo.2009.08.006

Giggenbach, W. F. (1992). Isotopic shifts in waters from geothermal and volcanic systems along convergent plate boundaries and their origin. *Earth Planet Sci. Lett.* 113, 495–510. doi:10.1016/0012-821X(92)90127-H

Goldsmith, J. R., Graf, D. L., Chodos, A. A., Joensuu, O. I., and Mcvicker, L. D. (1958). Relation between lattice constants and composition of Ca-Mg carbonates. *Am. Mineral.* 43, 84–101.

Greinert, J., Bohrmann, G., and Suess, E. (2001). "Gas hydrate-associated carbonates and methane-venting at hydrate ridge: classification, distribution, and origin of authigenic lithologies," in *Natural gas hydrates: occurrence, distribution, and detection* (Washington, DC: American Geophy-sical Union, 99–113.

Grossman, E. L., and Ku, T.-L. (1986). Oxygen and carbon isotope fractionation in biogenic aragonite: Temperature effects. *Chem. Geol. Isot. Geosci.* 59, 59–74. doi:10.1016/0168-9622(86)90057-6

Gründger, F., Carrier, V., Svenning, M. M., Panieri, G., Vonnahme, T. R., Klasek, S., et al. (2019). Methane-fuelled biofilms predominantly composed of methanotrophic ANME-1 in Arctic gas hydrate-related sediments. *Sci. Rep.* 9, 9725. doi:10.1038/s41598-019-46209-5

Guan, H., Feng, D., Wu, N., and Chen, D. (2016). Methane seepage intensities traced by biomarker patterns in authigenic carbonates from the South China Sea. *Org. Geochem.* 91, 109–119. doi:10.1016/j.orggeochem.2015.11.007

Guan, H., Sun, Z., Mao, S., Xu, L., Cao, H., and Geng, W. (2019). Authigenic carbonate formation revealed by lipid biomarker inventory at hydrocarbon seeps: A case study from the Okinawa Trough. *Mar. Petrol. Geol.* 101, 502–511.

Haas, A., Peckmann, J., Elvert, M., Sahling, H., and Bohrmann, G. (2010). Patterns of carbonate authigenesis at the Kouilou pockmarks on the Congo deep-sea fan. *Mar. Geol.* 268, 129–136. doi:10.1016/j.margeo.2009.10.027,2010

Han, Y. J., and Aizenberg, J. (2003). Effect of magnesium ions on oriented growth of calcite on carboxylic acid functionalized self-assembled monolayer. *J. Am. Chem. Soc.* 125, 4032–4033. doi:10.1021/ja034094z

Hesse, R. (2003). Pore water anomalies of submarine gas-hydrate zones as tool to assess hydrate abundance and distribution in the subsurface what have we learned in the past decade? *Earth Sci. Rev.* 61, 149–179. doi:10.1016/S0012-8252(02)00117-4

Hesse, R., and Harrison, W. E. (1981). Gas hydrates (clathrates) causing pore-water freshening and oxygen isotope fractionation in deep-water sedimentary sections of terrigenous continental margins. *Earth Planet Sci. Lett.* 55, 453–462. doi:10.1016/0012-821X(81)90172-2

Himmler, T., Birgel, D., Bayon, G., Pape, T., Ge, L., Bohrmann, G., et al. (2015). Formation of seep carbonates along the Makran convergent margin, northern Arabian Sea and a molecular and isotopic approach to constrain the carbon isotopic composition of parent methane. *Chem. Geol.* 415, 102–117. doi:10.1016/j.chemgeo.2015.09.016

Himmler, T., Sahy, D., Martma, T., Bohrmann, G., Plaza-Faverola, A., Bünz, S., et al. (2019). A 160,000-year-old history of tectonically controlled methane seepage in the Arctic. *Sci. Adv.* 5, eaaw1450. doi:10.1126/sciadv.aaw1450

Holler, T., Wegener, G., Knittel, K., Boetius, A., Brunner, B., Kuypers, M. M., et al. (2009). Substantial (13) C/(12) C and D/H fractionation during anaerobic oxidation of methane by marine consortia enriched *in vitro*. *Environ. Microbiol. Rep.* 1, 370–376. doi:10.1111/j.1758-2229.2009.00074.x

Hong, W. L., Torres, M. E., Carroll, J., Crémière, A., Panieri, G., Yao, H., et al. (2017). Seepage from an arctic shallow marine gas hydrate reservoir is insensitive to momentary ocean warming. *Nat. Commun.* 8, 15745. doi:10.1038/ncomms15745

Hong, W.-L., Torres, M. E., Portnov, A., Waage, M., Haley, B., and Lepland, A. (2018). Variations in gas and water pulses at an arctic seep: fluid sources and methane transport. *Geophys. Res. Lett.* 45, 4153. doi:10.1029/2018gl077309

James, R. H., Bousquet, P., Bussmann, I., Haeckel, M., Kipfer, R., Leifer, I., et al. (2016). Effects of climate change on methane emissions from seafloor sediments in the Arctic Ocean: A review. *Limnol. Oceanogr.* 61 (S1), S283–S299.

Kennett, J. P., Cannariato, K. G., Hendy, I. L., and Behl, R. J. (2000). Carbon isotopic evidence for methane hydrate instability during quaternary interstadials. *Science* 288, 128–133. doi:10.1126/science.288.5463.128

Kim, S.-T., O'Neil, J. R., Hillaire-Marcel, C., and Mucci, A. (2007). Oxygen isotope fractionation between synthetic aragonite and water: influence of temperature and Mg2+ concentration. *Geochem. Cosmochim. Acta* 71, 4704–4715. doi:10.1016/j.gca.2007.04.019

Knief, C. (2015). Diversity and habitat preferences of cultivated and uncultivated aerobic methanotrophic bacteria evaluated based on pmoA as molecular marker. *Front. Microbiol.* 6 (487), 1346. doi:10.3389/fmicb.2015.01346

Knies, J., Daszinnies, M., Plaza-Faverola, A., Chand, S., Sylta, Ø., Bünz, S., et al. (2018). Modelling persistent methane seepage offshore western Svalbard since

early Pleistocene. *Mar. Petrol. Geol.* 91, 800–811. doi:10.1016/j.marpetgeo.2018.01.020

Knittel, K., and Boetius, A. (2009). Anaerobic oxidation of methane: progress with an unknown process. *Annu. Rev. Microbiol.* 63, 311–334. doi:10.1146/annurev.micro.61.080706.093130

Knittel, K., Lösekann, T., Boetius, A., Kort, R., and Amann, R. (2005). Diversity and distribution of methanotrophic archaea at cold seeps. *Appl. Environ. Microbiol.* 71 (1), 467–479. doi:10.1128/AEM.71.1.467-479.2005

Krause, S., Niemann, H., and Treude, T. (2017). "Methane seeps in a changing climate." in *Life at vents and seeps*. Editor J. Kallmeyer (Berlin, Boston: De Gruyter), 1–32.

Lein, A. Y. (2004). Authigenic carbonate formation in the ocean. *Lithol. Miner. Resour.* 39 (1), 1–30. doi:10.1023/B:LIMI.0000010767.52720.8f

Lösekann, T., Knittel, K., Nadalig, T., Fuchs, B., Niemann, H., Boetius, A., et al. (2007). Diversity and abundance of aerobic and anaerobic methane oxidizers at the Haakon Mosby Mud Volcano, Barents Sea. *Appl. Environ. Microbiol.* 73 (10), 3348–3362.

Kim, S. -T., O'Neil„ J. R., Hillaire-Marcel, C., and Mucci, A. (2007). Oxygen isotope fractionation between synthetic aragonite and water: influence of temperature and Mg2+ concentration. Geochimica et Cosmochimica Acta. 71 (19), 4704–4715.

MacDonald, I. R., Guinasso, N. L., Jr., Sassen, R., Brooks, J. M., Lee, L., and Scott, K. T. (1994). Gas hydrate that breaches the sea floor on the continental slope of the Gulf of Mexico. *Geology* 22, 699–702. doi:10.1130/0091-7613

Mazzini, A., Ivanov, M. K., Parnell, J., Stadnitskaia, A., Cronin, B. T., Poludetkina, E., et al. (2004). Methane-related authigenic carbonates from the Black Sea: geochemical characterisation and relation to seeping fluids. *Mar. Geol.* 212, 153–181. doi:10.1016/j.margeo.2004.08.001

Milucka, J., Ferdelman, T. G., Polerecky, L., Franzke, D., Wegener, G., Schmid, M., et al. (2012). Zero-valent sulphur is a key intermediate in marine methane oxidation. *Nature* 491, 541–546. doi:10.1038/nature11656

Naehr, T. H., Eichhubl, P., Orphan, V. J., Hovland, M., Paull, C. K., Ussler, W., et al. (2007). Authigenic carbonate formation at hydrocarbon seeps in continental margin sediments: a comparative study. *Deep Sea Res. Part II Top. Stud. Oceanogr.* 54, 1268–1291. doi:10.1016/j.dsr2.2007.04.010

Natalicchio, M., Peckmann, J., Birgel, D., and Kiel, S. (2015). Seep deposits from northern Istria, Croatia: a first glimpse into the Eocene seep fauna of the Tethys region. *Geol. Mag.* 152, 444–459. doi:10.1017/S0016756814000466

Niemann, H., Duarte, J., Hensen, C., Omoregie, E., Magalhães, V. H., Elvert, M., et al. (2006). Microbial methane turnover at mud volcanoes of the gulf of Cadiz. *Geochem. Cosmochim. Acta* 70 (21), 5336–5355. doi:10.1016/j.gca.2006.08.010

Niemann, H., and Elvert, M. (2008). Diagnostic lipid biomarker and stable carbon isotope signatures of microbial communities mediating the anaerobic oxidation of methane with sulphate. *Org. Geochem.* 39, 1668–1677. doi:10.1016/j.orggeochem.2007.11.003

Niemann, H., Elvert, M., Hovland, M., Orcutt, B., Judd, A., Suck, I., et al. (2005). Methane emission and consumption at a North Sea gas seep (Tommeliten area). *Biogeosciences* 2, 335–351. doi:10.5194/bg-2-335-2005

Panieri, G., Bünz, S., Fornari, D. J., Escartin, J., Serov, P., Jansson, P., et al. (2017). An integrated view of the methane system in the pockmarks at Vestnesa Ridge, 79°N. *Mar. Geol.* 390, 282–300. doi:10.1016/j.margeo.2017.06.006

Pape, T., Bünz, S., Hong, W.-L., Torres, M. E., Riedel, M., Panieri, G., et al. (2020). Origin and transformation of light hydrocarbons ascending at an active pockmark on Vestnesa Ridge, Arctic Ocean. *J. Geophys. Res.: Solid Earth* 125, e2018JB016679. doi:10.1029/2018jb016679

Peckmann, J., Birgel, D., and Kiel, S. (2009). Molecular fossils reveal fluid composition and flow intensity at a Cretaceous seep. *Geology* 37, 847–850. doi:10.1130/G25658A.1

Peckmann, J., and Thiel, V. (2004). Carbon cycling at ancient methane-seeps. *Chem. Geol.* 205, 443–467. doi:10.1016/j.chemgeo.2003.12.025

Plaza-Faverola, A., Bünz, S., Johnson, J. E., Chand, S., Knies, J., Mienert, J., et al. (2015). Role of tectonic stress in seepage evolution along the gas hydrate-charged Vestnesa Ridge, Fram Strait. *Geophys. Res. Lett.* 42, 733–742. doi:10.1002/2014gl062474

Presley, B. J., and Kaplan, I. R. (1968). Changes in dissolved sulfate, calcium and carbonate from interstitial water of near-shore sediments. *Geochem. Cosmochim. Acta* 32, 1037–1048. doi:10.1016/0016-7037(68)90106-3

Reitner, J., Peckmann, J., Blumenberg, M., Michaelis, W., Reimer, A., and Thiel, V. (2005). Concretionary methane-seep carbonates and associated microbial communities in Black Sea sediments. *Palaeogeogr. Palaeoclimatol. Palaeoecol* 227, 18–30. doi:10.1016/j.palaeo.2005.04.033

Reeburgh, W. S. (2007). Oceanic methane biogeochemistry. *Chem. Rev*, 107, 486–513.

Sauer, S., Crémière, A., Knies, J., Lepland, A., Sahy, D., Martma, T., et al. (2017). U-Th chronology and formation controls of methane-derived authigenic carbonates from the Hola trough seep area, northern Norway. *Chem. Geol.* 470, 164–179. doi:10.1016/j.chemgeo.2017.09.004

Sauer, S., Hong, W. L., Yao, H., Knies, J., Lepalnd, A., Klug, M., et al. (2020). Methane transport and sources in an Arctic deep-water cold seep offshore NW Svalbard (Vestnesa Ridge, 79°N). *Deep Sea Res. Part I: Oceanogr. Res. Papers* 167, 103430. doi:10.1016/j.dsr.2020.103430

Sen, A., Åström, E. K. L., Hong, W.-L., Portnov, A., Waage, M., Serov, P., et al. (2018a). Geophysical and geochemical controls on the megafaunal community of a high Arctic cold seep. *Biogeosci. Discuss.* 15, 4533–4559. doi:10.5194/bg-15-4533-2018

Sen, A., Duperron, S., Hourdez, S., Piquet, B., Léger, N., Gebruk, A., et al. (2018b). Cryptic frenulates are the dominant chemosymbiotrophic fauna at Arctic and high latitude Atlantic cold seeps. *PloS One* 13 (12), e0209273. doi:10.1371/journal.pone.0209273

Serov, P., Vadakkepuliyambatta, S., Mienert, J., Patton, H., Portnov, A., Silyakova, A., et al. (2017). Postglacial response of Arctic Ocean gas hydrates to climatic amelioration. *Proc. Natl. Acad. Sci. U. S. A.* 114 (24), 6215–6220. doi:10.1073/pnas.1619288114

Steinle, L., Graves, C. A., Treude, T., Ferré, B., Biastoch, A., Bussmann, I., et al. (2015). Water column methanotrophy controlled by a rapid oceanographic switch. *Nat. Geosci.* 8 (5), 378–382.

Steinle, L., Schmidt, M., Bryant, L., Haeckel, M., Linke, P., Sommer, S., et al. (2016). Linked sediment and water-column methanotrophy at a man-made gas blowout in the North Sea: implications for methane budgeting in seasonally stratified shallow seas. *Limnol. Oceanogr.* 61 (S1), S367–S386.

Ussler, W., and Paull, C. K. (1995). Effects of ion exclusion and isotopic fractionation on pore water geochemistry during gas hydrate formation and decomposition. *Geo Mar. Lett.* 15, 37–44. doi:10.1007/BF01204496

van Grinsven, S., Damsté, J. S. S., Asbun, A. A., Engelmann, J. C., Harrison, J., and Villanueva, L. (2020a). Methane oxidation in anoxic lake water stimulated by nitrate and sulfate addition. *Environ. Microbiol.* 22 (2), 766–782. doi:10.1111/1462-2920.14886

van Grinsven, S., Damsté, J. S. S., Harrison, J., and Villanueva, L. (2020b). Impact of electron acceptor availability on methane-influenced microorganisms in an enrichment culture obtained from a stratified lake. *Front. Microbiol.* 11, 403. doi:10.3389/fmicb.2020.00715

Wegener, G., Krukenberg, V., Riedel, D., Tegetmeyer, H. E., and Boetius, A. (2015). Intercellular wiring enables electron transfer between methanotrophic archaea and bacteria. *Nature* 526, 587–590. doi:10.1038/nature15733

Whiticar, M. J. (1999). Carbon and hydrogen isotope systematics of bacterial formation and oxidation of methane. *Chem. Geol.* 161 (1-3), 291–314. doi:10.1016/S0009-2541(99)00092-3

Yao, H., Hong, W. L., Panieri, G., Sauer, S., Torres, M. E., Lehmann, M. F., et al. (2019). Fracture-controlled fluid transport supports microbial methane-oxidizing communities at Vestnesa Ridge. *Biogeosciences* 16, 2221–2232. doi:10.5194/bg-16-2221-2019

Yao, H., Niemann, H., and Panieri, G. (2020). Multi-proxy aproach to unravel methane emission history of an Arctic cold seep. *Quat. Sci. Rev.* 244, 106490.

Conflict of Interest: The authors declare that the research was conducted in the absence of any commercial or financial relationships that could be construed as a potential conflict of interest.